

# Mitigation of Discrete Spectral Components in Filtered BPSK and OQPSK Signals

Victor A. Vilnrotter\* and Dennis K. Lee\*

**ABSTRACT.** — Telemetry received from deep-space or near-Earth spacecraft often contains strong discrete spectral components extending far beyond the main lobe of the continuous spectrum. This is attributed to filtering of the data-modulated phase in the spacecraft transmitter, which generates discrete spectral components in the spectra of transmitted binary phase-shift keying (BPSK), quadrature phase-shift keying (QPSK), and offset quadrature phase-shift keying (OQPSK) modulations. The theoretical development and simulations in this article focus on BPSK and OQPSK modulations, due to the underlying compatibility in the techniques used to mitigate discrete spectral components. The reasons for the appearance of spectral lines in BPSK and OQPSK modulations are examined, and methods designed to eliminate discrete spectral components are proposed and evaluated. Finally, the practical limits imposed by finite-phase modulator bandwidth is addressed, and its impact on achievable data rate examined.

## I. Introduction

Adjacent channel interference can occur when multiple spacecraft are simultaneously present in the receiving antenna's field of view. Spacecraft transponders employ a phase modulator that converts voltage to phase in order to modulate the signal onto the carrier, thus maintaining a constant envelope signal. The modulation format most commonly employed in the past for low to moderate data rate communications in the deep-space and near-Earth environments is binary phase-shift keying, or BPSK. BPSK is a one-dimensional signal constellation capable of error-free communication at data rates commensurate with the available bandwidth  $B$ , namely at a rate  $R \cong B$  bits/s. With a given bandwidth constraint, higher data rates can be achieved by resorting to higher-dimensional signals such as quadrature phase-shift keying (QPSK) and a modification of QPSK known as offset quadrature phase-shift keying (OQPSK) [1,2,3]. Although the mathematical descriptions of QPSK and OQPSK signals are similar, the techniques developed in this article to mitigate discrete spectral components are better suited to BPSK and OQPSK signals, hence we focus on mitigation techniques for these two modulation formats.

---

\* Communications Architectures and Research Section.

The research described in this publication was carried out by the Jet Propulsion Laboratory, California Institute of Technology, under a contract with the National Aeronautics and Space Administration. © 2017 California Institute of Technology. U.S. Government sponsorship acknowledged.

When ideal square pulses are used to represent the data symbols, the spectra of BPSK, QPSK, and OQPSK are continuous, free of discrete components. However, the spectra of square pulses extend to high frequencies, hence with a bandwidth constraint the square pulses will necessarily be filtered at the highest data rates supported by the available bandwidth. When filtered pulses are applied to the phase modulator, discrete components begin to appear in the spectra, with magnitude proportional to the amount of pulse distortion due to filtering, as discussed in [1].

Examples of discrete components in the spectra of spacecraft signals received from the Mars Reconnaissance Orbiter (MRO) are shown in Figure 1, resulting from filtered BPSK and QPSK signals. The discrete components can be seen to extend to high frequencies in both cases, potentially causing interference in adjacent channel signals. In this article, a detailed analysis of the causes for the occurrence of discrete components in a practical system is presented. Algorithms designed to reduce or eliminate the discrete components in BPSK and OQPSK spectra are proposed and evaluated, using realistic simulations to illustrate the results.

## II. Phase-Modulated Downlink Signals

Our primary interest is the spectrum of the transmitted signal, particularly the large discrete components far from the main lobe, that could potentially interfere with signals in adjacent channels. For our purposes, an estimate of the spectrum of the modulated carrier can be obtained as an average of the squared magnitude of its Fourier transform,  $\mathcal{F}\{s(t)\} = \int s(t) \exp(-j2\pi ft) dt$ . Since the spectrum of the modulated carrier is just a frequency-shifted version of the complex envelope, it is sufficient to estimate the spectrum of the complex envelope,  $\exp\{j[\theta_m \varphi(t)]\}$ . This is the approach we take in this article, focusing on the spectrum of the complex envelope in order to determine the spectral response of the modulated carrier.

Phase modulation is applied to the quadrature channel with intensity controlled by a parameter called the modulation index,  $\theta_m$ , with the rest of the power allocated to the residual carrier in the in-phase channel. With  $\theta_m = \pi/2$ , the carrier component is completely eliminated, hence this case is referred to as the “suppressed carrier” modulation. With  $0 \leq \theta_m < \pi/2$ , some power is relegated to the carrier, hence this case is called “residual carrier” modulation. The transmitted signal  $s(t)$  can be represented as the real part of the complex envelope  $\tilde{s}(t) = \sqrt{P} \exp\{j[\theta_m \varphi(t)]\} = \sqrt{P} (\cos[\theta_m \varphi(t)] + j \sin[\theta_m \varphi(t)])$  multiplied by a phasor representing the complex carrier,  $\exp(j\omega_0 t)$ , resulting in

$$s(t) = \sqrt{P} \operatorname{Re} \left( \exp\{j[\theta_m \varphi(t)]\} \exp(j\omega_0 t) \right) = \sqrt{P} \cos[\omega_0 t + \theta_m \varphi(t)],$$

where  $\omega_0 = 2\pi f_0$  is the carrier radian frequency,  $t$  is time (representing either continuous or oversampled discrete samples),  $P$  is the power of the transmitted signal (constant for an ideal square pulse), and  $\varphi(t)$  is the symbol modulation. Note that  $\operatorname{Re}\{\tilde{s}(t)\} = \operatorname{Re}(\sqrt{P} \exp\{j[\omega_0 t + \theta_m \varphi(t)]\}) = \sqrt{P} \cos[\omega_0 t + \theta_m \varphi(t)]$  contains both the I and Q components of the complex envelope, as can be seen by expanding the cosine

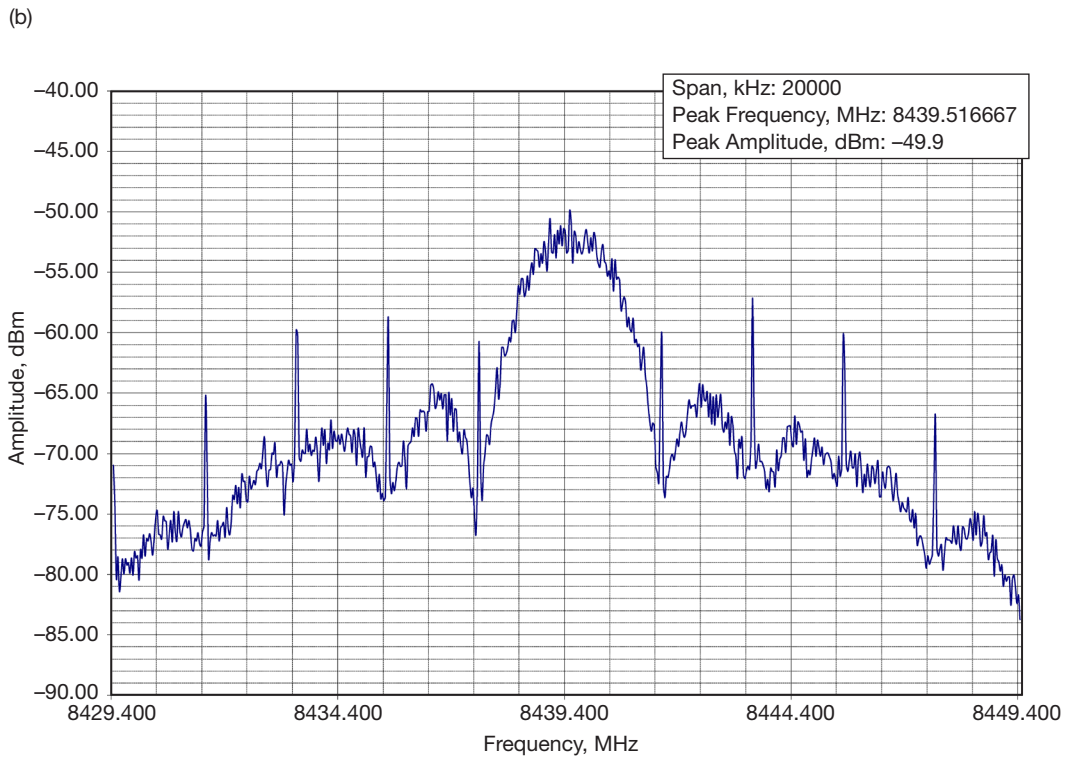
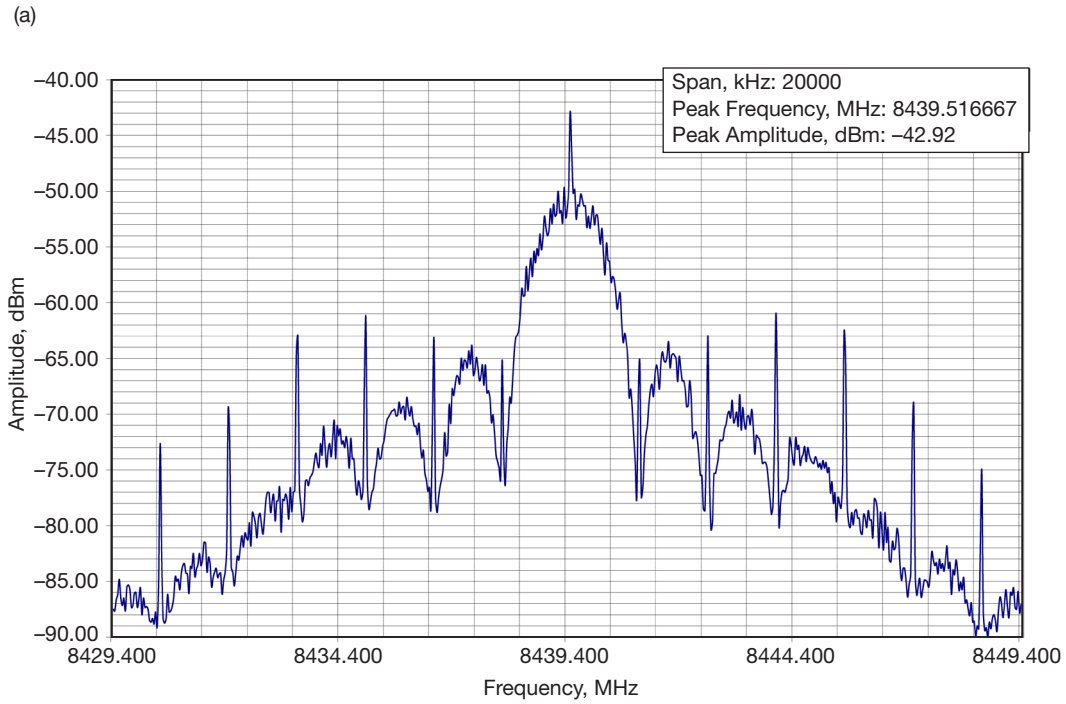


**Figure 1. Spectra of signals received from the Mars Reconnaissance Orbiter spacecraft, showing large discrete components at the nulls of the continuous spectrum, with (a) filtered-phase BPSK modulation, and (b) filtered-phase QPSK modulation.**

term as  $\cos[\omega_0 t + \theta_m \varphi(t)] = \cos(\omega_0 t) \cos[\theta_m \varphi(t)] - \sin(\omega_0 t) \sin[\theta_m \varphi(t)]$ , where  $\cos(\omega_0 t)$  and  $\sin(\omega_0 t)$  represent the I and Q components, respectively. Hence, modulating the phase of the complex envelope results in a real signal that contains both the real and the imaginary components of the complex envelope superimposed on the carrier waveform. We begin the development of mitigation techniques for discrete spectral components with the simplest case, namely, BPSK modulation.

#### A. Time Series and Complex-Plane Representation of BPSK Modulation

BPSK is an accepted modulation format used extensively for both deep-space and near-Earth communications. Ideal BPSK modulation consists of a binary data sequence  $\{d_k \in (0, 1)\}$ , mapped to a set of non-return-to-zero (NRZ) voltages  $\{a_k \in (-1, 1)\}$ , scaled by the modulation index  $\theta_m$  and applied to a sequence of rectangular pulses  $p_0(t)$  of duration  $T$  seconds. In the absence of filtering, the BPSK phase modulation sequence can be expressed as  $\varphi(t) = \sum_k a_k p_0(t - kT)$ . An example of BPSK phase modulation sequence corresponding to the data sequence  $d_k = 10110101\dots$  is shown in Figure 2 for the case  $\theta_m = \pi/2$ .

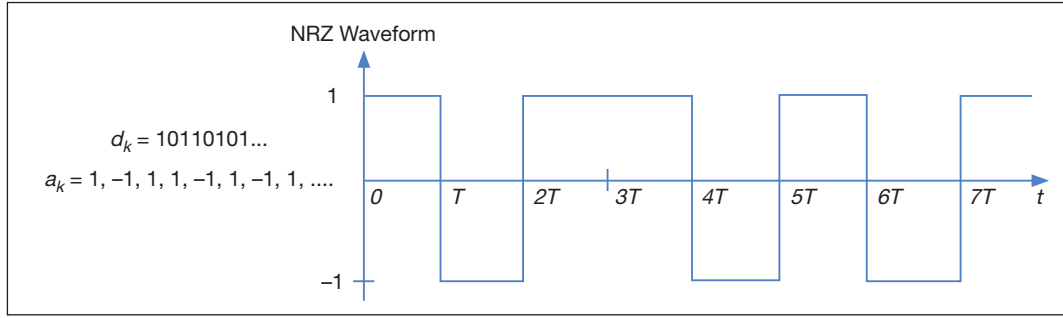


**Figure 2. Example of BPSK modulation sequence: binary data stream  $\{d_k \in (0, 1)\}$  converted to two-level symbols  $\{a_k \in (-1, 1)\}$ , generating the sequence  $\varphi(t) = \sum_k a_k p_0(t - kT)$ .**

The BPSK phase modulation sequence  $\varphi(t)$  is scaled by the modulation index  $\theta_m$  and converted to a complex envelope process  $\tilde{s}(t)$  via complex exponentiation:

$$\tilde{s}(t) = \exp[j\theta_m \varphi(t)] = \exp\left[j\theta_m \sum_k a_k p_0(t - kT)\right]. \quad (1)$$

Finally, the complex envelope modulates a microwave carrier of radian frequency  $\omega_0$  via multiplication by the complex phasor  $\exp(j\omega_0 t)$ . Taking the real part of  $\tilde{s}(t)$  and scaling it by the square root of the spacecraft power  $P$  forms the real physical signal  $s(t)$  that propagates through space to the receiver:

$$\begin{aligned} s(t) &= \sqrt{P} \operatorname{Re}\{\exp(j\omega_0 t) \tilde{s}(t)\} \\ &= \sqrt{P} \operatorname{Re}\{\exp[j\omega_0 t + \theta_m \varphi(t)]\} \\ &= \sqrt{P} \cos\left[\omega_0 t + \theta_m \sum_k a_k p_0(t - kT)\right]. \end{aligned} \quad (2)$$

When the pulses are filtered, the phase process can be expressed as  $\varphi(t) = \theta_m \sum_k a_k p(t - kT)$ , where  $p(t) = p_0(t) \otimes h(t)$  represents the filtered version of the square pulses  $p_0(t)$ , filtered by the frequency-domain impulse response  $h(t)$ , and where  $\otimes$  denotes convolution. Examples of filtered (dashed red) and unfiltered (solid blue) pulse streams, converted to phase via the modulation index  $\theta_m = \pi/2 = 1.571$ , are shown in Figure 3.

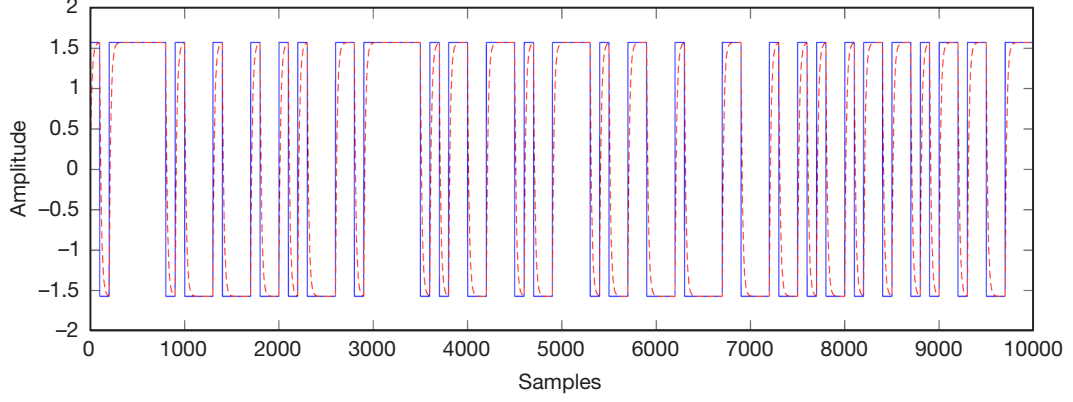


**Figure 3. Example of a filtered (dashed red) and unfiltered (solid blue) binary phase stream, with wideband first-order Butterworth filtering and modulation index  $\theta_m = \pi/2$ .**

#### Time-Series Model

It is clear that the complex envelope  $\tilde{s}(t)$  contains all the information needed to specify the power spectrum of the signal, since complex multiplication by  $\exp(j\omega_0 t)$  simply shifts the baseband spectrum to the carrier frequency  $\omega_0$ . Therefore, the complex envelope  $\tilde{s}(t)$  will be used to determine the baseband signal spectra in the rest of this article. Although continuous-time notation will be used, this model applies to sampled waveforms as well, provided that each symbol is sampled at a rate much greater than the Nyquist rate.

The complex envelope can be expressed in terms of in-phase and quadrature components using Euler's identity,  $\exp(j\theta) = \cos(\theta) + j\sin(\theta)$ . Applying Euler's identity to the complex envelope yields the following representation:

$$\begin{aligned} \tilde{s}(t) &= \exp[j\theta_m \varphi(t)] = \cos[\theta_m \varphi(t)] + j\sin[\theta_m \varphi(t)] \\ &= \cos\left[\theta_m \sum_k a_k p_0(t - kT)\right] + j\sin\left[\theta_m \sum_k a_k p_0(t - kT)\right] \\ &\equiv s_I(t) + js_Q(t) \end{aligned} \quad (3)$$

where  $s_I(t) = \cos[\theta_m \varphi(t)]$  is the in-phase component, and similarly  $s_Q(t) = \sin[\theta_m \varphi(t)]$  is the quadrature component. With  $a_k = \pm 1$ ,  $\theta_m = \pi/2$ ,  $p_0(t)$  an ideal square pulse, and recognizing that  $\cos(\pm\pi/2) = 0$ , the expression for the complex envelope in Equation (3) becomes

$$\tilde{s}(t) = j\sin[\theta_m \varphi(t)] = j\sin\left[\theta_m \sum_k a_k p_0(t - kT)\right] = js_Q(t). \quad (4)$$

The I and Q components for the unfiltered pulses are illustrated in Figure 4(a) for the case  $\theta_m = \pi/2$ , showing that the modulation is contained entirely in the quadrature component (magenta) since the in-phase component (light blue) is zero when  $\theta_m = \pi/2$ . The Euler identity is satisfied at each point because the quadrature component changes sign instantaneously for the case of ideal square pulses,  $\exp[j\frac{\pi}{2}\varphi(t)] = \cos[\frac{\pi}{2}\varphi(t)] + j\sin[\frac{\pi}{2}\varphi(t)]$ ; hence the Euler identity is satisfied with  $s_I(t) = \cos[\frac{\pi}{2}\varphi(t)] = 0$  when  $\varphi(t) = \sum_k a_k p_0(t - kT)$  and  $a_k = \pm 1$ .

When the phase process is filtered, the quadrature waveform cannot change sign instantaneously due to the finite-bandwidth impulse response  $h(t)$ , as shown by the magenta component in Figure 4(b), hence the in-phase component must be non-zero in the transition regions to satisfy the Euler identity. The non-zero response of the in-phase component is shown in Figure 4(b) as positive-going (blue) pulses occurring each time the quadrature component changes sign. The key to understanding the non-zero response of the in-phase component in Figure 4(b) is to realize that when the filtered phase function  $\varphi(t)$  moves from  $-\frac{\pi}{2}$  to  $+\frac{\pi}{2}$ , or equivalently the Q component  $\sin[\varphi(t)]$  increases from  $-1$  to  $+1$ , the I component  $\cos[\varphi(t)]$  first increases from zero to  $+1$  and then decreases to zero, since  $\cos[\varphi(t)] \geq 0$  when  $-\frac{\pi}{2} \leq \varphi(t) \leq \frac{\pi}{2}$ . The same argument holds as the Q component decreases from  $+1$  to  $-1$ ; therefore, the I component always increases from zero to  $+1$  as the Q component changes sign in either direction. Note that in a sampled implementation, the Euler identity must be satisfied at each sample; however, the signal trajectory between samples does not contribute to the sampled response.

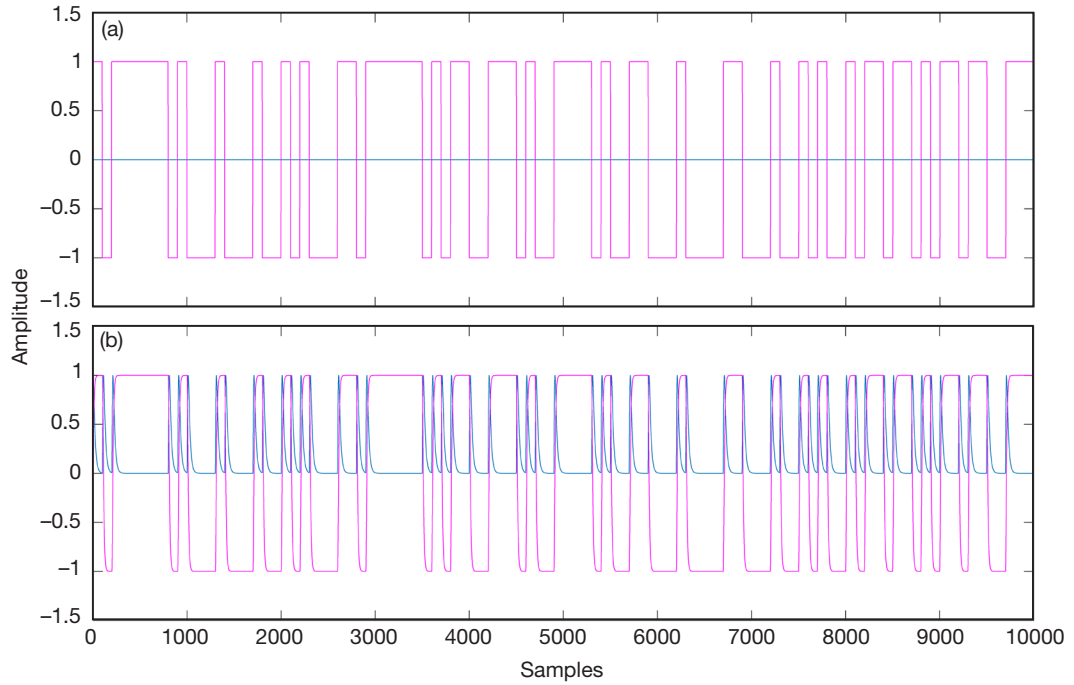


**Figure 4. BPSK modulation: (a) I (blue) and Q (magenta) waveforms with unfiltered (infinite-bandwidth) pulses; (b) I and Q waveforms with filtered pulses.**

### Complex Plane Model

The time-series model developed above helps to describe the signal path in the complex plane, which is particularly useful for explaining the behavior of the signal spectra, and of the algorithms designed to mitigate discrete components in the spectrum. Figure 5(a) is a zoomed-in version of Figure 4(a), showing the trajectory of the modulation at a transition where the quadrature signal amplitude changes from +1 to -1, represented by the successive points A and B. The phase changes from  $+\pi/2$  to  $-\pi/2$  from one sample to the next, which in this digital representation implies an instantaneous (or effectively infinite bandwidth) transition. As the signal jumps from point A to point B instantaneously, or more precisely in less than one sample-interval, the in-phase or cosine component remains zero throughout the transition, hence the quadrature component can be viewed as remaining entirely on the imaginary axis during the jump.

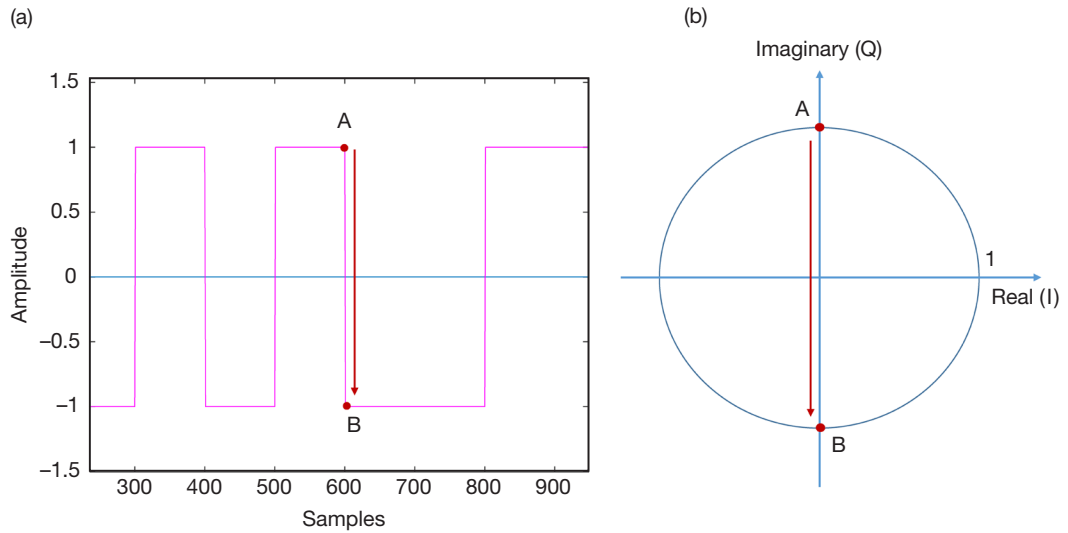


**Figure 5. (a) Zoomed version of Figure 3(a), showing transition from point A to point B; (b) complex-plane interpretation of the A–B transition with wideband phase modulator.**

When the phase function  $\varphi(t)$  is filtered, as shown by the dashed red lines in the example of Figure 3, the I component must take on non-zero values for samples after point A as the filtered Q component approaches point B, since filtering has reduced the bandwidth of the phase function to the point that the transition from point A to point B must take more than one sample to complete.

The application of Euler's identity is illustrated in the filtered responses of Figure 6, which shows the I and Q components as functions of time, as well as the trajectory of the phasor along the unit circle in the complex plane. Consistent with the conclusion of the time-series model described above, the non-zero temporal response of the Q component after filtering generates positive-going pulses in the I component with effective duration corresponding to the impulse response of the filter.

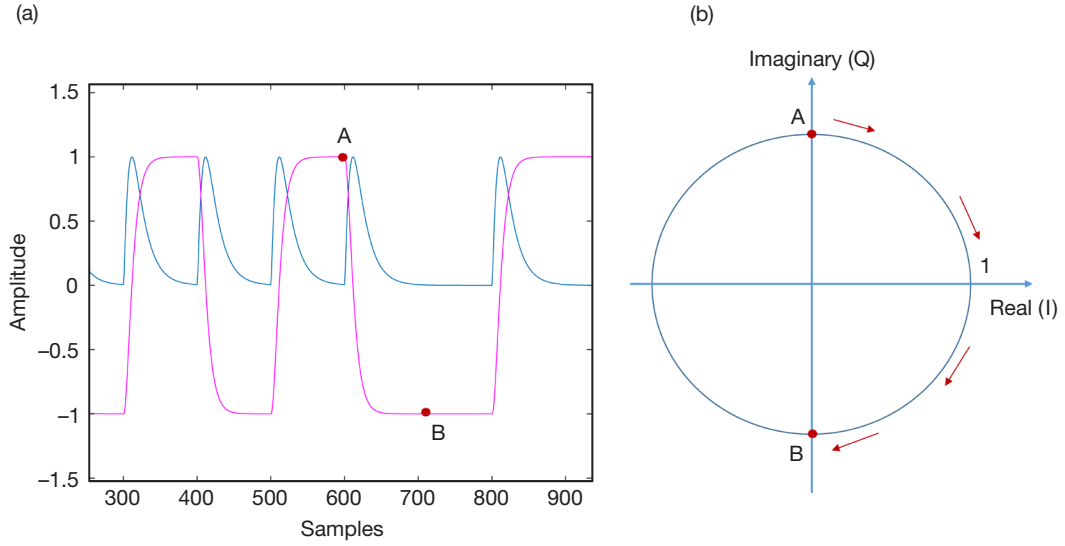


**Figure 6. (a) Zoomed version of Figure 4(b), showing filtered I and Q response from point A to point B; (b) complex-plane interpretation of the A-B transition with narrowband (filtered) phase modulator.**

#### Power Spectral Density of BPSK, QPSK, and OQPSK with Unfiltered Pulses

The power spectral density of square-pulse (unfiltered)  $T$ -second BPSK modulated symbols,  $S_{BPSK}(f)$ , is given by the well-known formula [1]:

$$S_{BPSK}(f) = \left| \int_0^T e^{-j2\pi ft} dt \right|^2 = T \left( \frac{\sin(\pi fT)}{\pi fT} \right)^2. \quad (5)$$

The first zero of the main lobe occurs at frequency  $1/T$  Hz, hence filtering to suitable multiples of this bandwidth enables communication at a data rate of  $R_{BPSK} = 1/T$  symbols per second, with symbols of  $T$ -second duration.

The power spectra of ideal unfiltered QPSK and OQPSK are the same as that of unfiltered BPSK:

$$S_{QPSK}(f) = S_{OQPSK}(f) = \left| \int_0^T e^{-j2\pi ft} dt \right|^2 = T \left( \frac{\sin(\pi fT)}{\pi fT} \right)^2 = S_{BPSK}, \quad (6)$$

hence the bandwidth requirements are the same as that of BPSK. However, the throughput for QPSK becomes  $R_{QPSK} = 2/T$  symbols per second, or twice that of BPSK. If  $2T$ -second substream symbols are employed, then the main lobe width of the power spectrum becomes half that of BPSK,

$$S_{QPSK}(f) = 2T \left( \frac{\sin(2\pi fT)}{2\pi fT} \right)^2,$$

with first zero at  $1/2T$  Hz and data throughput  $R_{QPSK} = 1/T$ , equal to that of BPSK.



It can be seen that the power spectra of unfiltered BPSK, QPSK, and OQPSK are continuous, without any discrete spectral components. However, for the case of filtered phase modulation, the power spectrum is considerably more complicated to derive, as described in [1], hence we employ a simpler approach to evaluate the power spectral densities of filtered modulations and strategies designed to mitigate discrete components.

The Fourier transform of the continuous representation of the complex envelope,  $\tilde{s}(f) \equiv \mathcal{F}\{\tilde{s}(t)\}$ , can be expressed as

$$\begin{aligned}\tilde{s}(f) &\equiv \mathcal{F}\{\tilde{s}(t)\} = \int_{-\infty}^{\infty} \tilde{s}(t) \exp(j\omega t) dt \\ &= \int_{-\infty}^{\infty} s_I(t) \exp(j\omega t) dt + j \int_{-\infty}^{\infty} s_Q(t) \exp(j\omega t) dt \equiv \tilde{S}_I(f) + \tilde{S}_Q(f),\end{aligned}\quad (7)$$

where we made use of the Euler representation of the complex envelope, namely  $\tilde{s}(t) = s_I(t) + js_Q(t)$ . It can be seen that the Fourier transform can be expressed as the sum of components due to the  $I$  and the  $Q$  waveforms,  $\tilde{S}_I(f)$  and  $\tilde{S}_Q(f)$ , respectively, hence if the  $I$  component is zero, then the Fourier transform of the complex envelope reduces to  $\tilde{S}_Q(f)$ . When the BPSK symbols are filtered, resulting in positive-going pulses in the  $I$  component, then both  $I$  and  $Q$  Fourier transforms contribute to the power spectrum.

An estimate of the spectrum of the complex envelope can be obtained by computing the fast Fourier transform (FFT) of the symbol stream over a large number of symbols, and taking the squared magnitude of the resulting FFT. This approach yields  $|\tilde{S}_1(f)|^2$  as the initial estimate of the power spectrum of BPSK in the simplified continuous-time notation. This initial estimate tends to generate large random fluctuations in the frequency domain, hence it is customary to average a large number  $N$  of spectral estimates, using independent data sequences, to reduce the fluctuations in the estimate, yielding the average estimate of the power spectrum as

$$\hat{P}_S = \frac{1}{N} \sum_{i=1}^N |\tilde{S}_i(f)|^2.$$

This is called a periodogram, an example of which is shown in Figure 7, where  $N = 100$  independent estimates were averaged to obtain the final results.

#### Power Spectral Density of Filtered BPSK Pulses

The blue curve in Figure 7 represents the spectrum of unfiltered BPSK data phase-modulated onto the complex envelope. As expected, the simulated unfiltered pulses generate the continuous BPSK spectrum as defined in Equation (5). When the phase function  $\varphi(t)$  is filtered as shown by the dashed red lines in Figure 3, the in-phase component takes on non-zero values between points A and B due to the filtering operation, as shown in Figure 6(a). It is clear that the  $I$  and  $Q$  components are projections of the phasor onto the real and imaginary axes, as the signals propagate from point A to point B.

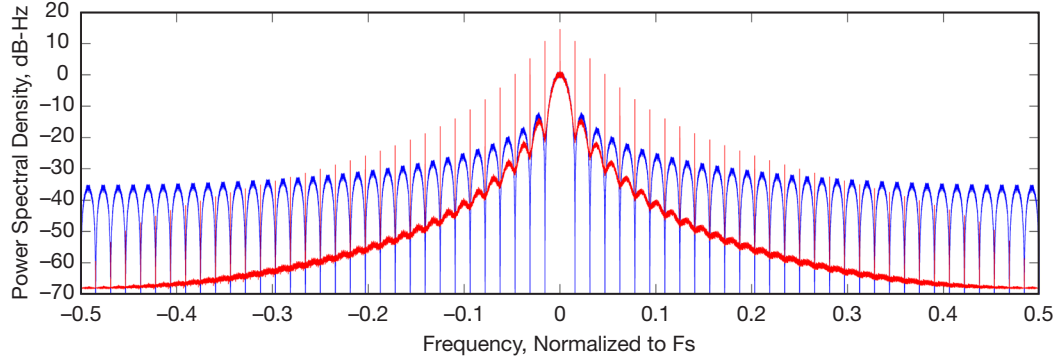


**Figure 7. Power spectral densities of unfiltered (blue) and phase-filtered BPSK pulses, showing the emergence of discrete components due to phase filtering.**

The impact of positive-going I component pulses on the spectrum is shown in Figure 7 as the red curve, where the discrete spectral components can be seen evenly spaced at frequencies of integral multiples of  $1/T$ , as expected from a train of periodic pulses in the I component. The discrete spectral components remain even if the positive-going pulses are thinned by randomly nulling the pulses where runs of zeros or ones occur in the data, as shown in Figure 6(a) at point B. The effect of thinning is to reduce the power in the discrete components; however, a thinned pulse-train still correlates with a fundamental Fourier component at frequency  $1/T$ , resulting in discrete spectral components, albeit at reduced power level.

### **III. Mitigation Strategies Designed to Reduce Discrete Components in the Transmitted Spectrum**

Four different mitigation techniques were developed to reduce or eliminate unwanted discrete spectral components in the transmitted spectrum: these techniques are designated as Methods 1–4. However, Method 1 applies only to BPSK, while Methods 2–4 apply to OQPSK modulation, even though some of the underlying concepts are similar. Modifications are necessary because filtered OQPSK cannot be decomposed into independent BPSK data streams modulated onto the I and Q components, as in the unfiltered case, hence mitigation techniques developed for BPSK cannot be applied directly to OQPSK signals. In short, Method 1 is a “toggled phase” approach designed specifically for filtered BPSK modulation; Method 2 applies a modified version of Method 1 to filtered OQPSK modulation by replacing “toggled phase” with “unwrapped phase” in the mitigation algorithm. Method 3 sets upper and lower limits for the unwrapped phase, and reflects the evolving phase function from these predetermined boundaries in order to limit the maximal phase excursions. Finally, Method 4 reduces phase excursions by estimating and subtracting the slowly varying trend from the unwrapped phase. These four mitigation techniques are examined and evaluated in the following sections.

#### **Method 1: BPSK Modulation with Unwrapped and Toggled Phase**

A plausible approach to eliminating discrete spectral components due to positive-going pulses in the I component, as described above, is to alternately add  $\pi$  radians to the modu-

lation index, alternately placing the center of the phase modulation at  $\pi$  radians instead of zero. This results in alternating positive- and negative-going pulses, as shown in Figure 8(a), and hence the path from A to B is switched to the left half of the complex plane, as shown in Figure 8(b).

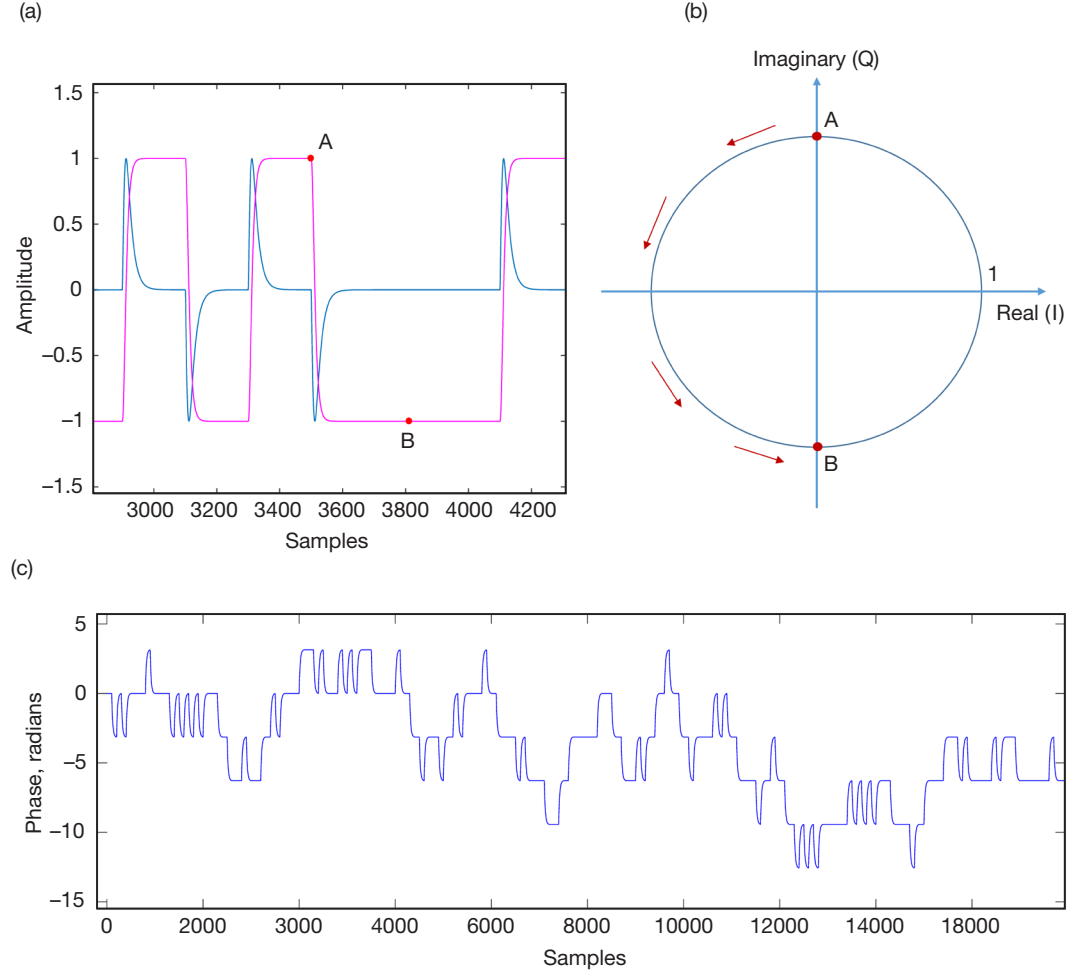


**Figure 8. (a) Alternating I component pulses, resulting from altering the phase center between 0 and  $\pi$  radians; (b) complex-plane trajectory of A–B transition when phase center is switched from 0 to  $\pi$  radians; (c) example of phase waveform of “toggled” BPSK modulation after filtering.**

This mitigation strategy can be accomplished by employing the following operations: (1) multiply the random (0,1) data stream by an alternating 1,-1,1,-1,... “square-wave” sequence; (2) accumulate the resulting “toggled” data stream, and convert it to a sampled waveform approximating the continuous-time signal. After multiplication by twice the modulation index  $2\theta_m = \pi$ , effectively toggling the phase between 0 and  $\pi$  instead of  $\pm\pi/2$ , this operation results in a phase waveform resembling a random walk with  $\pi$  radian steps, as shown in Figure 8(c) for the case of filtered BPSK pulses.

The spectrum of the complex envelope phase-modulated by the unwrapped waveform shows no evidence of discrete spectral components, as can be seen in Figure 9 (red curve).

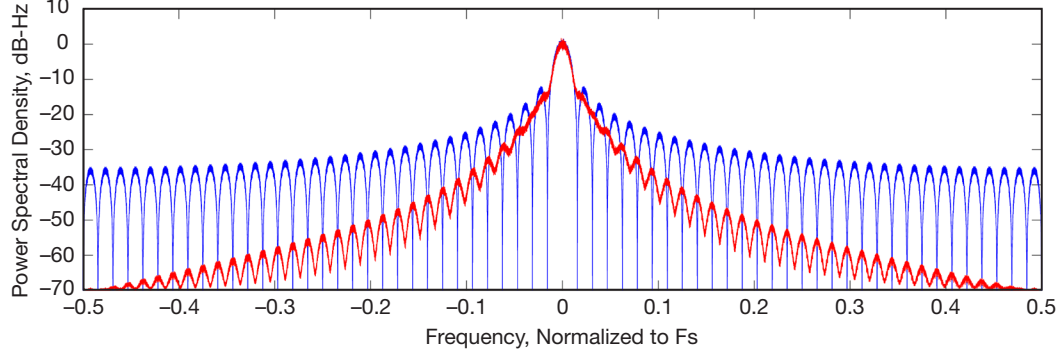


**Figure 9. Spectrum of unfiltered BPSK symbols (blue) and spectrum of filtered, phase-center toggled BPSK symbols (red).**

The blue curve is the spectrum of the complex envelope modulated by the unfiltered square waveform. It can be seen that toggling eliminates the discrete spectral components for the unfiltered case. Note, however, that the toggling operation can lead to arbitrarily large phase values, which can exceed the limits of practical phase modulators.

The reason for the elimination of the discrete components (or “spikes”) in the spectrum can be explained by noting that the spikes in the spectrum of filtered BPSK are caused by positive-going pulses. After applying the toggling operation, the I component can be partitioned into positive and negative pulses:  $s_I(t) = s_I^+(t) + s_I^-(t)$ , where for each pulse  $s_I^-(t) = -s_I^+(t)$ . The discrete components in the spectrum are the Fourier transforms of the I component, which can likewise be partitioned into “+” and “-” components:  $\tilde{S}_I(f) = \mathcal{F}\{s_I^+(t) + s_I^-(t)\} = \tilde{S}_I^+(f) + \tilde{S}_I^-(f)$ , where  $\tilde{S}_I^-(f) = -\tilde{S}_I^+(f)$ . On the average, there are an equal number of positive- and negative-going pulses in the I component with random data. Since the Fourier transform is an averaging operation over a large number of samples for each frequency component, the expected value of the discrete spectrum can be expressed as the sum of two components,  $E[\tilde{S}_I(f)] = E[\tilde{S}_I^+(f) + \tilde{S}_I^-(f)] = E[\tilde{S}_I^+(f)] + E[\tilde{S}_I^-(f)] = 0$ , hence the discrete components disappear when the toggling operation is applied to BPSK data. The filtered spectrum resulting from toggling the phase center of filtered BPSK is shown in Figure 9 as the red curve, demonstrating that the discrete spectral components have been eliminated via the phase-center toggling strategy.

#### **A. Time Series and Complex-Plane Representation of OQPSK Modulation**

OQPSK is a modified version of QPSK signaling where one of the subcomponents is shifted in time by half a symbol duration, or  $T/2$  seconds, thereby limiting the phase shift to 90 deg when symbol transitions occur. It has the same throughput rate as QPSK and the same power spectrum, since shifting one of the substreams by  $T/2$  seconds is simply a time delay, which corresponds to a phase-shift term in the transform domain that does not impact the power spectrum.

It is clear from the unfiltered BPSK model that only the Q component is modulated, while the I component is zero with suppressed carrier modulation: in other words, when

$\theta_m = \pi/2$ . With QPSK modulation, both the I and Q components are modulated, enabling communication at twice the data rate of BPSK without sacrificing bandwidth (but with some degradation in detection performance at low signal-to-noise ratios).

With OQPSK modulation, the (0,1) data bits are grouped into consecutive pairs, where each pair of binary symbols represents a quaternary symbol that can take on any of four values: 00, 01, 10, 11. The components of each binary substream are converted to NRZ symbols via the mapping  $(0,0) \rightarrow (-1, -1), (0,1) \rightarrow (1, 1), (1,0) \rightarrow (1, -1), (1,1) \rightarrow (-1, 1)$ .

Note that an alternate mapping with inverted signs can also be used, without any impact on the results. Next, two data streams are generated by assigning the first NRZ symbol to the “odd” data stream, and the second to the “even” data stream, and delaying one of the data streams by half a symbol duration, or  $T/2$  seconds, relative to the other. An example of the partitioned OQPSK symbol streams is shown in Figure 10(a), where the odd symbol stream is represented by blue lines, and the even symbol stream by dashed red lines, as a function of time in the continuous model but here represented by samples.

Figure 10(b) is a close-up or zoomed view of the two symbol streams, showing that the two symbol streams are offset by half a symbol duration, which implies that during any transition only one of the symbols can change sign. This further implies that the phase can only

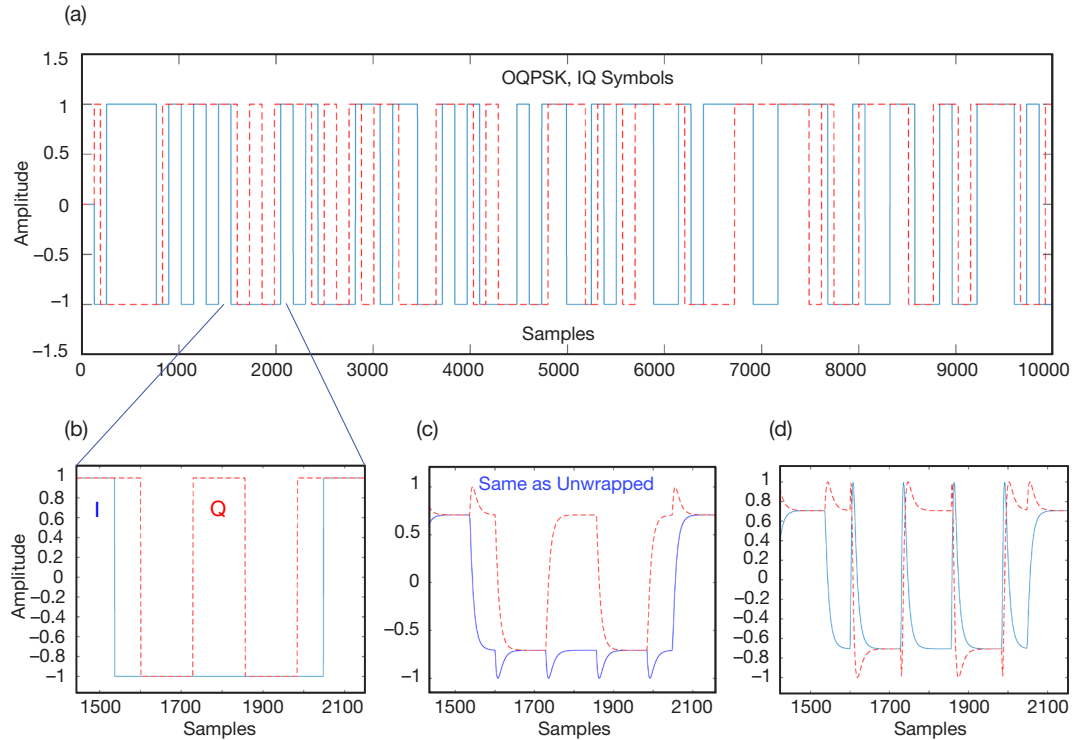


**Figure 10. (a) Unfiltered odd (dashed red) and even (blue) data streams modulated onto I and Q components of OQPSK signal; (b) zoomed version of unfiltered data stream, illustrating  $T/2$  second offset; (c) unwrapped, filtered, mod- $2\pi$  version of zoomed section; (d) filtered, mod- $2\pi$  version of zoomed section, illustrating large spikes in the I component when unwrapping is not applied before filtering.**

change by  $\pi/2$  radians, as opposed to QPSK symbols where the phase can change by either  $\pi/2$  or  $\pi$  radians during a transition. Figure 10(c) is the unwrapped, filtered version of the zoomed data symbols shown in Figure 10(b) after the mod- $2\pi$  operation, while Figure 10(d) illustrates the fundamentally different response when the phase is not unwrapped prior to filtering.

Note that while unfiltered OQPSK data streams can be represented as independent BPSK data streams modulated onto the I and Q components, phase-filtered OQPSK data streams cannot be decomposed in this manner due to the dependence in the phase introduced by the filtering operation. In addition, transmitters that employ phase filtering typically modulate the filtered phase waveform directly onto the carrier for transmission without any further signal processing. Therefore, Method 1 cannot be applied directly to the I and Q data streams to reduce the power in the discrete components, hence different mitigation approaches are needed for OQPSK modulation. The following three approaches, designated Methods 2, 3, and 4, describe techniques designed to mitigate discrete spectral components with phase-filtered OQPSK modulation.

#### Method 2: Unwrapping the OQPSK Phase Before Filtering

As the phase transits from one state to another, the phasor rotates on the unit circle either clockwise or counterclockwise at any given time in accordance with the random binary data stream. Since the odd and even waveforms are staggered in time by  $T/2$ , the I and Q components transition alternately every  $T/2$  seconds (however, there may be no transition if the data remain the same from one bit to the next). If the phasor rotates from  $7\pi/4$  to  $\pi/4$  by crossing the positive real line in the counterclockwise direction, it actually accumulates  $2\pi$  radians during this transition, so this end-point should be called  $9\pi/4$  instead of  $\pi/4$ . Here the idea is that if we keep track of the number of complete revolutions of the phasor over the unit circle, then we can “unwrap” the phase and eliminate jumps of  $2\pi$  radians when the real line is crossed. This is equivalent to the “unwrapped and toggled” phase described in the section on BPSK modulations, except with OQPSK symbols the toggling operation is not necessary, since the OQPSK phasor can rotate into either the left or right half of the complex plane depending on the succession of binary data symbols, whereas with BPSK (without toggling) the rotation is confined to the right-half plane.

#### Analysis of Difference Between “Wrapped” and “Unwrapped” OQPSK Phase

The difference between the spectra when “wrapped” and “unwrapped” phases are used is critical when symbol filtering is involved. Conventional phase limited to  $\pm\pi$  (or  $0 - 2\pi$ ) radians is designated as “wrapped” phase, whereas absolute phase without limits is called “unwrapped” phase. In the following analysis, we assume that the response of the phase modulator is instantaneous, hence the phase modulator can respond to a  $2\pi$  radian change in a single sample without distortion. This idealized assumption will be relaxed in the last section, where the impact of finite-phase modulator bandwidth will be investigated.

## Time-Series Analysis

The green plot in Figure 11(a) is an example of the “unwrapped,” unfiltered OQPSK phase trajectory, expressed in radians. The blue plot is the filtered, “unwrapped” phase modulo  $2\pi$  and the red curve is the filtered “wrapped” (modulo  $2\pi$ ) phase. The dashed gray lines indicate the  $(+\pi, -\pi)$  boundaries, which is just a more symmetric representation of the modulo  $2\pi$  boundaries.

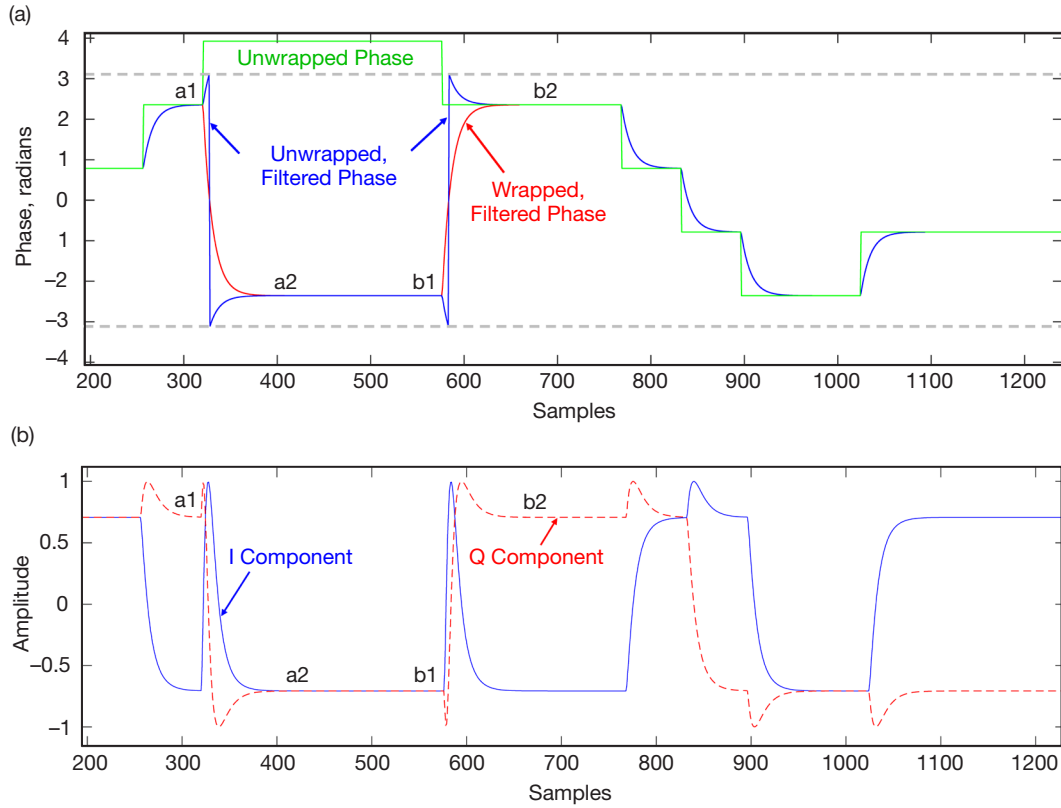


**Figure 11. (a) Wrapped and unwrapped phase functions for filtered OQPSK symbols, illustrating behavior at transitions; (b) in-phase and quadrature components corresponding to the filtered phase function.**

As the unwrapped (green) phase crosses the  $+\pi$  boundary upwards in a single sample at the point a1, the filtered unwrapped modulo  $2\pi$  phase (blue) also proceeds upward at a1 towards the upper boundary at  $\pi$  radians, until reaching the sample point closest to  $\pi$  from below: the next sample is just above  $\pi$ , hence the modulo  $2\pi$  operation subtracts  $2\pi$  from the unwrapped value, yielding the next sample point just above the lower boundary of  $-\pi$ . Therefore, the unwrapped (green) and unwrapped-filtered-modulo- $2\pi$  (blue) phases both proceed in the positive direction towards the sample point a2. Similarly, the green and blue phases proceed in the same downward direction at the point b1, with a similar modulo  $2\pi$  transition for the blue curve at the  $-\pi$  boundary.

The phase trajectory is very different for the wrapped-filtered-modulo- $2\pi$  phase (red curve). When the unwrapped (green) curve is wrapped modulo  $2\pi$ , the consecutive sample points before and after a1 change abruptly from  $+\pi/4$  radians ( $+135$  deg) to  $-\pi/4$  radians ( $-135$  deg) in a single step. When this rapid downward transition is filtered, the resulting

red curve shown in Figure 11(a) proceeds in a downward direction towards  $a_2$ , not in the upward direction as was the case with the green and blue curves. Therefore, the wrapped and filtered phase (red curve) proceeds in the opposite direction from the unwrapped and filtered phase (blue curve), which leads to very different responses in the I and Q components for these two cases.

Figure 11(b) shows the corresponding IQ components for the wrapped filtered (red) phase, near the same set of points. Since the red curve proceeds in the downward direction at  $a_1$  towards  $a_2$ , namely from  $+135$  deg to  $+90$  deg to  $0$  deg, then continuing to  $-90$  and  $-135$  deg, it follows that the Q component (proportional to the sine of the phase) first increases from  $0.707$  at  $a_1$  to  $+1$ , then decreases to  $0$ ,  $-1$ , and finally settles at  $-0.707$  at  $a_2$ , as shown by the dashed red curve in Figure 11(b). At the same time, the I component (proportional to the cosine of the phase) starts out at  $-0.707$  at  $+135$  deg ( $a_1$ ), proceeds upward to  $0$  at  $+90$  deg, then to  $+1$  at  $0$  deg, followed by  $0$  at  $-90$  deg, finally settling at  $-0.707$  upon reaching  $a_2$  at  $-135$  deg.

Similarly, the wrapped filtered phase in Figure 11(a) is proceeding in the upward direction at the point  $b_1$ , leading to a negative-positive-negative-going Q component during the transition from  $b_1$  to  $b_2$ , which is opposite to the  $a_1$ – $a_2$  transition. However, the I component again results in a positive-going spike, as can be seen in Figure 11(b). Therefore, the I component of the wrapped filtered phase yields positive-going spikes located at integral numbers of  $T$ -second symbol durations: this, in turn, generates discrete spectral components in the spectrum of the wrapped filtered phase, as can be seen in Figure 13.

### Complex-Plane Analysis

It is instructive to examine the above concepts in the context of complex-plane analysis, which provides further insights into the key issues differentiating wrapped and unwrapped phase processing. Consider the response of the I and Q components in Figure 12(a), representing the signal path over the points A–B–C with unwrapped phase, or equivalently over the complex-plane path  $(-1, -1) \rightarrow (-1, 1) \rightarrow (-1, -1)$  in Figure 12(b). Starting at point A, the I component (blue) starts going negative from  $-0.707$  to  $-1$ , then back to  $-0.707$  as it reaches point B, while the Q component increases monotonically from  $-0.707$  to  $0.707$ : this is equivalent to tracing out the phasor from A–B in Figure 12(b), or equivalently the direct path from  $(-1, -1)$  to  $(-1, 1)$ . Similarly, the path B–C retraces the phasor directly from  $(-1, 1)$  to  $(-1, -1)$ . This response corresponds to the red spectrum in Figure 14: there are no discrete components, since there are approximately an equal number of small negative- and positive-going pulses as the I and Q phasors rotate through maxima on the real and imaginary axes.

The response of the I and Q components for the wrapped and filtered case is depicted in Figure 12(c). The large positive-going spike as the I component traverses from A to B implies that the phasor travels counterclockwise through  $+1$  on the real axis as shown in Figure 12(d), then back again the long way. The large positive-going spikes on a  $T$ -second support give rise to the discrete components at multiples of  $1/T$  Hz in the red spectrum in Figure 13.



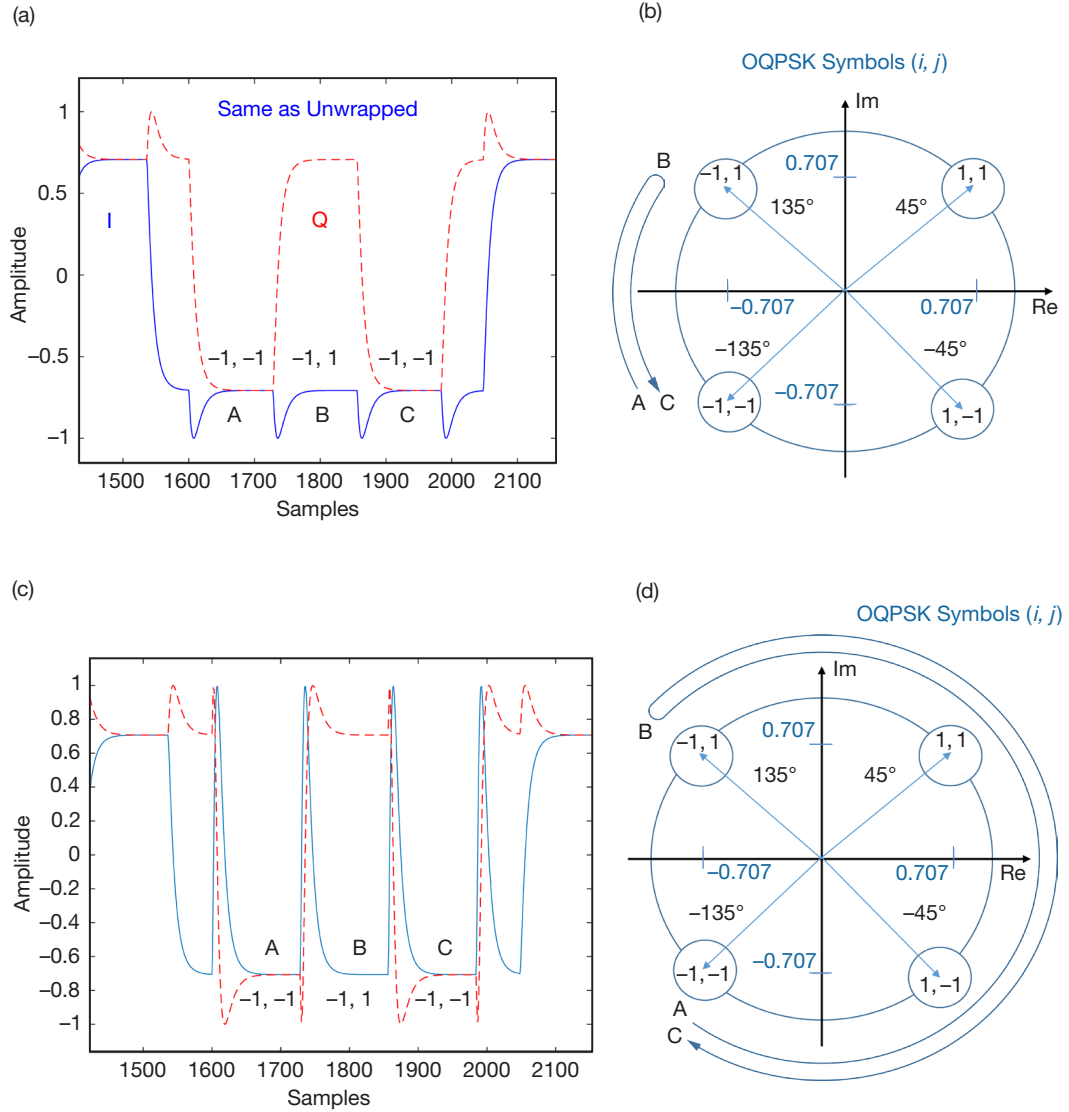


**Figure 12. (a) Time-series plot of unwrapped OQPSK in-phase and quadrature components; (b) complex-plane representation of phasor trajectory for unwrapped OQPSK phase; (c) time-series plot of wrapped OQPSK in-phase and quadrature components; (d) complex-plane representation of phasor trajectory for wrapped OQPSK phase.**

However, the unwrapped filtered phase does not generate any spikes, because even after filtering the direction of the phase remains consistent with the unwrapped phase, hence the phasor is able to reverse direction at the  $\pm\pi$  boundaries, and the positive-going spikes are not generated in the I component with this approach. The result is that large spikes in the spectrum are completely eliminated, as shown in Figure 14.

As discussed above, filtering of unwrapped phase does not produce spikes in the spectrum, because the I and Q components are able to transition the 180-deg boundary between the  $(-1, 1)$  and  $(-1, -1)$  states directly, hence do not generate periodic spikes in the positive direction in the time domain, which would lead to discrete components in the spectrum.

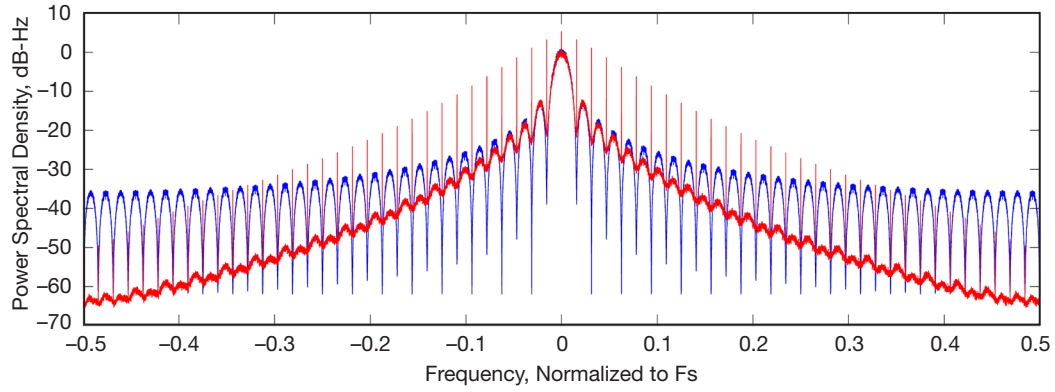


**Figure 13. Spectrum of ideal OQPSK (blue) and spectrum of wrapped, filtered-phase OQPSK (red).**

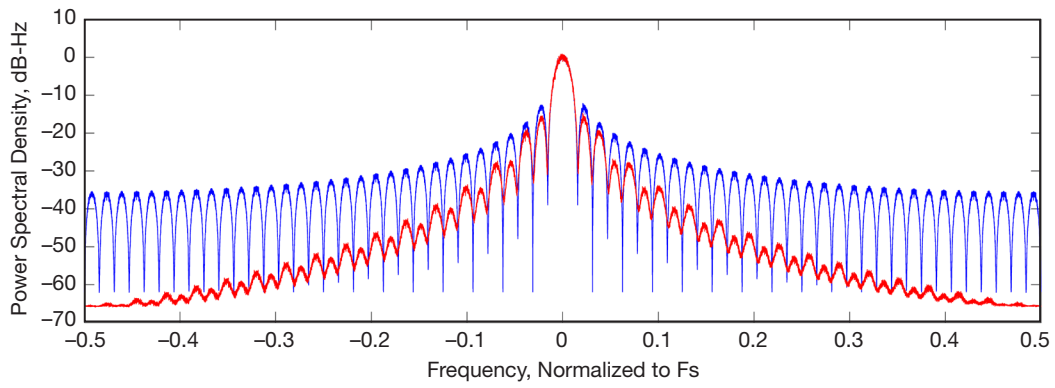


**Figure 14. Spectrum of ideal unfiltered OQPSK phase (blue) and spectrum of unwrapped, filtered and modulo  $2\pi$  phase (red).**

The above results are predicated on the assumption of infinite modulator bandwidth, and hence apply approximately when the bandwidth of the phase modulator is much greater than the symbol bandwidth. If this assumption is not valid, then additional spikes can occur in the spectrum, as discussed in a subsequent section.

#### Method 3: Reflected, Filtered, Unwrapped OQPSK Phase

Next, we consider an approach designed to limit the phase excursions of the unwrapped OQPSK phase by reflecting the phase function at predetermined boundaries, selected to meet the voltage requirements of the cascaded phase modulators.

We have seen that unwrapping the phase waveform eliminates the discrete spectral components in the filtered case. However, this approach has practical limits, because in a physical implementation the phase must be converted to a voltage and applied to a practical phase modulator to generate a modulated carrier suitable for transmission. Since the unwrapped phase can reach arbitrarily large values, it is clear that arbitrarily large voltages would be required to fully implement the unwrapped phase modulation, which is not practical. Therefore, the unwrapped phase must be limited to practical voltage levels in a realistic physical system. The required voltage limiting can be achieved by effectively wrapping the

phase around an integer multiple of the phase,  $2\pi K$ , where  $K$  is an integer selected to accommodate the voltage limits of a cascade of  $K$  physical phase modulators.

In a given vector of  $M$  symbols, there can be at most  $M/\lceil 2\pi K/(\pi/2) \rceil = M/4K$  reflections, but this maximal number occurs only when the unwrapped phase is moving rapidly in one direction, which is unlikely with random data. It was found that with  $K = 2$ , most phase vectors of length 1000 symbols that were used in the simulations generated many fewer reflections than the maximum number of  $1000/8 = 125$ . Examples of a typical unwrapped phase vector (magenta) and its reflected version (blue) are shown in Figure 15(a), where 128 samples per symbol are used to represent each of 1000 filtered symbols. The unwrapped phase shows relatively small phase excursions in the first 30,000 samples and in the last 40,000 samples where relatively few reflections occurred, while the middle 58,000 samples show greater excursions and hence require more reflections to contain the phase within  $\pm 2\pi$  radians. Figure 15(b) is a zoomed version of the first 20,000 reflected samples, where comparison with Figure 15(a) shows that eight reflections were required to contain the unwrapped filtered phase within the  $\pm 2\pi$  boundaries used in this example.

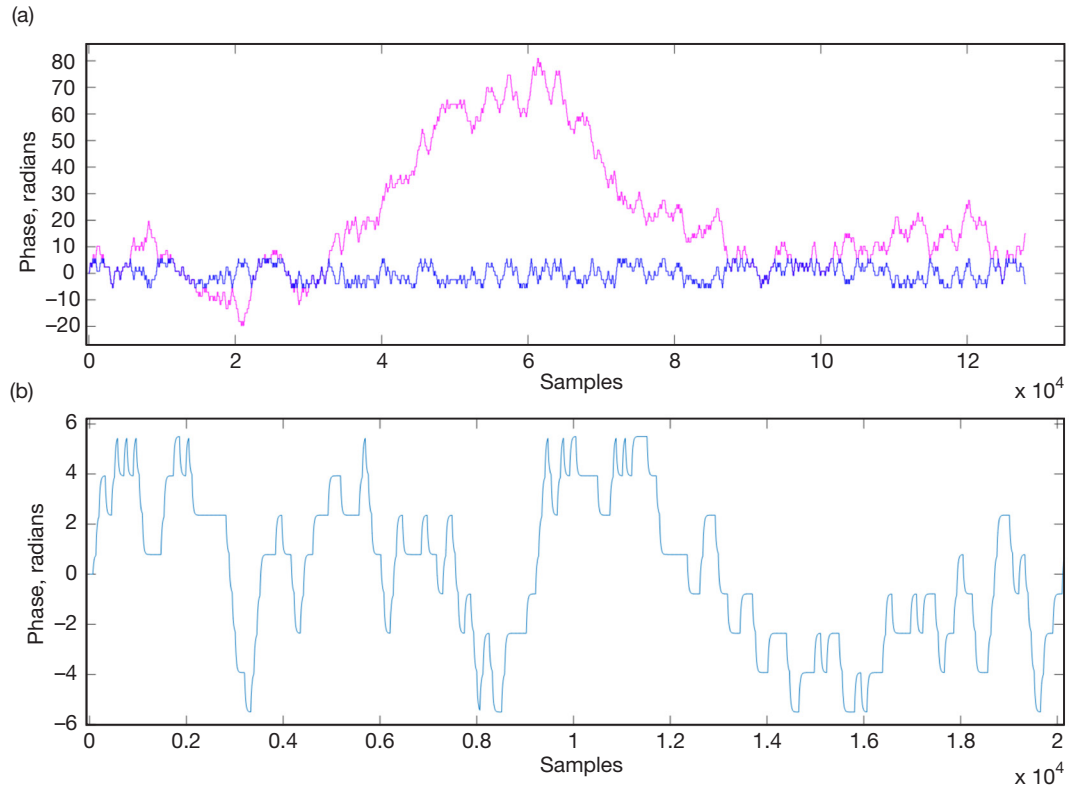


**Figure 15. (a) Unwrapped OQPSK phase (magenta) and phase reflected at  $\pm 2\pi$  boundaries; (b) zoomed version of the first 20,000 samples of unwrapped reflected filtered phase.**

An immediate consequence of Method 3 considered here (unwrapped phase reflected at specified  $2\pi K$  boundaries) is that the receiver must be able to determine where the reflections take place in the received signal, either as side information transmitted along with the signal (approximately 10 percent overhead required), or by using some form of traceback

technique at the receiver to determine the correct decoding path. The first approach increases complexity at the transmitter, since the location of the times where reflections took place must be included in the downlink data. However, since the data rate is typically wide-band compared to the trend of the unwrapped phase, the additional overhead (estimated at 10 percent) may be acceptable. The traceback technique at the receiver does not require any additional overhead at the transmitter; however, it will increase receiver complexity significantly, and may also impact receiver performance during low-SNR reception conditions.

The IQ components generated by the reflected unwrapped phase are shown in Figure 16, indicating numerous cases of positive-going spikes from  $-0.7$  to  $+0.7$  radians, three of which can be seen within the first 1000 samples. These positive-going spikes lead to discrete spectral components in the spectrum of the reflected-phase modulation. The spectrum of the reflected phase is shown in Figure 17 as the red curve, where it can be seen that the reflection operation results in small spikes at the even nulls of the continuous spectrum, but more analysis is needed to determine the reason why reflections at  $2\pi K$  boundaries result in spikes at the even nulls of the spectrum. However, the levels of the spikes in the unwrapped reflected phase spectrum are significantly smaller than the spikes in the wrapped OQPSK spectrum, as shown by direct comparison with Figure 13.

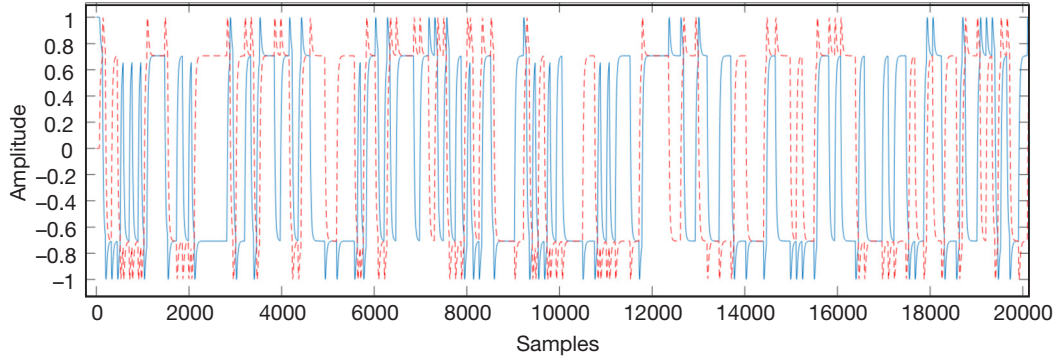


**Figure 16. In-phase (blue) and quadrature (dashed red) components of unwrapped OQPSK phase reflected at the boundaries.**

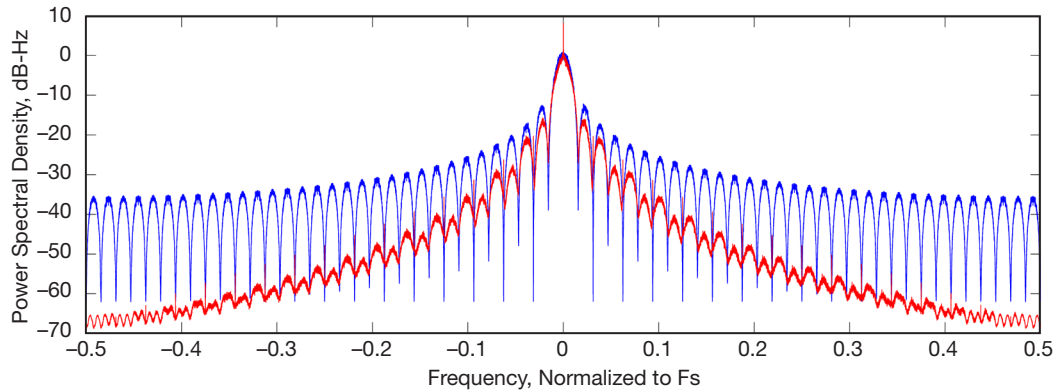


**Figure 17. Spectrum of ideal unfiltered OQPSK phase (blue) and spectrum of unwrapped, filtered and reflected OQPSK phase (red) showing discrete components at the even nulls of the continuous spectrum.**

#### Method 4: Unwrapped Filtered OQPSK Phase with Detrending

An alternate approach to eliminating the discrete spectral components in the spectrum due to periodic components in the I and Q components is based on the observation that if the unwrapped phase can be contained within  $2\pi K$  radians, then it is not necessary to apply the modulo  $2\pi$  operation to the unwrapped filtered phase, and hence the spectral spikes would disappear.

Since the binary data sequence generated by the sensors aboard the spacecraft is known before entering the phase modulator, in principle it is possible to evaluate the unwrapped phase process in advance, and adapt a narrowband lowpass filter to track the relatively slow trend in the random-walk process generated by the unwrapped phase. The trend can be removed from the unwrapped phase before inputting it to the phase modulator, generating in effect a “detrended” phase process with greatly reduced phase, and hence voltage excursions. Furthermore, the parameters of the narrowband lowpass filter can be adjusted adaptively to accommodate the rate of change of the trend, thus minimizing the phase excursions of the unwrapped filtered phase to accommodate the physical voltage limits of the modulator, or cascade of  $K$  modulators.

The key ideas of this approach are illustrated in Figure 18, where the blue curve is the unwrapped filtered phase, the green curve is the slowly varying trend, and the black curve is the difference of the two. Note that the black curve, which is the detrended version of the filtered unwrapped phase, is contained within much narrower limits than the unwrapped (blue) phase. The detrending operation alters the symbol response of the filtered phase, because the slow trend subtracted out or added into each symbol interval modifies the phase. Since the trend is slow compared to the symbol duration, the distortion is typically not significant. The symbol boundaries are preserved by the detrending operation, hence symbol synchronization should not be greatly affected; however, the full impact of detrending on OQPSK symbol detection remains to be investigated.

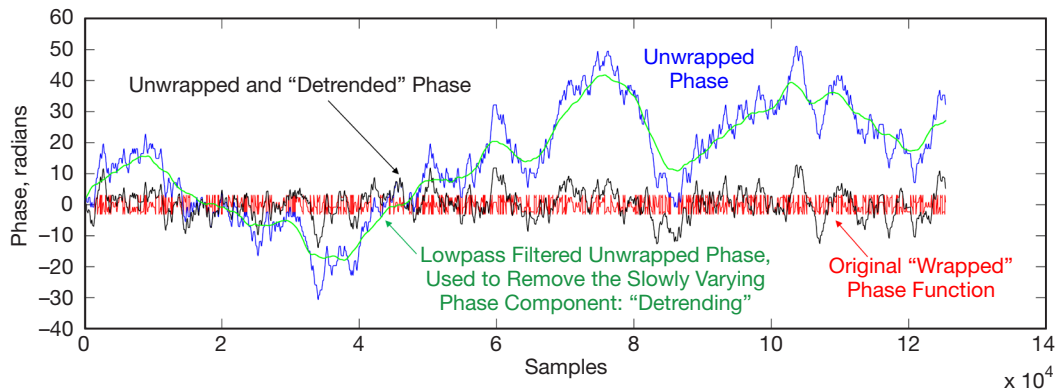


**Figure 18. Unwrapped and detrended phase function (black), with unwrapped phase (blue) and narrowband detrending function (green). The original “wrapped” phase is shown in red.**

In contrast to the detrended unwrapped phase shown by the black curve in Figure 18, the red curve represents the modulo  $2\pi$  version of the OQPSK phase, which is the conventional way to apply the filtered phase to the modulator (as described above). This “wrapped” phase is contained entirely in  $\pm\pi$  radians, hence can be accommodated with a single modulator, but it does give rise to periodic spikes in the I and Q components, as described earlier, which in turn give rise to large spikes in the spectrum, as shown in Figure 13.

The impact of the detrending operation on the OQPSK spectrum is significant, as shown by the red spectrum in Figure 19, where the discrete spectral components have been eliminated. It should also be noted that detrending does not involve a modulo  $2\pi$  operation after filtering, hence it is not subject to the restriction of near-instantaneous modulator response, as is the case with Method 2. Although it cannot be guaranteed that detrending will always contain the unwrapped phase entirely within the limits of the cascaded phase modulators, due to the random nature of the unwrapped phase, any occasional excursions outside the limits can be reflected using the technique described in Method 3. Although the reflection method does lead to small spikes in the spectrum, as shown above, the combination of detrending and reflection reduces the discrete spectral components below the levels shown in Figure 13, hence this approach may represent a practical way to eliminate spectral components in the transmitted OQPSK signals, provided the modulator bandwidth is much greater than the symbol bandwidth.

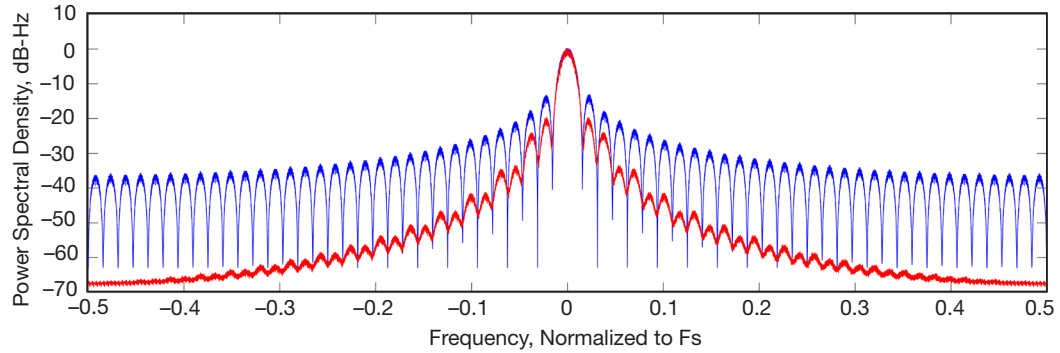


**Figure 19. Spectrum of phase-filtered OQPSK with unwrapped and detrended phase (red).**

#### Impact of Finite-Phase Modulator Bandwidth

A simulation has been implemented that takes into account the finite response time of the phase modulator by applying a wideband lowpass filter to the modulo  $2\pi K$  waveform, thus converting the instantaneous (one sample) jump into a slower response requiring several samples to complete the jump. A first-order lowpass filter with time constant  $\tau$  and impulse response  $h(t) = \tau \exp(-t/\tau)$  was applied to the sampled symbols to simulate the response of the modulator, before filtering the symbols with a much narrower first-order Butterworth lowpass filter with normalized corner frequency  $W_n/2 = 0.1$ . The corner frequency associated with the time constant  $\tau$  is  $B = 1/\tau$ . The Butterworth filter parameter  $W_n = 1$  corresponds to full sample bandwidth filtering, implying essentially infinite bandwidth or equivalently

instantaneous modulator response. The finite response time of modulators currently used in spacecraft can be approximated by a wideband lowpass filter with corner frequency of approximately 20 MHz, or a sampling rate of at least 40 MSPS in order to reconstruct the sampled waveform without distortion. When the modulator response is instantaneous, the sampled version of the phase waveform corresponds to the continuous waveform at the sample points, as shown by point a1 in Figure 20(a). This results in undistorted phase, and hence undistorted I and Q waveforms that do not generate discrete spectral components. However, when the phase waveform is filtered, even with a wideband but not infinite-bandwidth filter, as is the case with real physical modulators, the samples do not correspond exactly to the continuous waveform, as shown by the point a2 in Figure 20(a). This results in small glitches in the I and Q waveforms, as shown in Figure 20(b), where small spikes can be seen in the I and Q components at the samples where the phase waveform changes phase from  $+\pi$  to  $-\pi$ , in order to satisfy the Euler equality. The spikes in the Q component occur at the point where the Q component passes through zero phase, with alternating sign corresponding to the direction of the phase waveform, hence do not generate discrete components in the spectrum. However, the spikes in the I waveform are always in the positive direction, and since these spikes occur at a regular spacing (even when thinned), the spikes in the I waveform generate discrete spectral components, as can be seen in Figure 20(c). The time constant was set to  $\tau = 0.33$  for this case, implying that the second sample of the impulse response is not zero (as should be the case for infinite bandwidth), but rather a fraction  $\exp(-1/\tau) = \exp(-3) = 0.05$  of the peak, which distorts the phase waveform significantly at points of rapid change.

From the above analysis, it appears that the mitigation techniques for reducing spikes in the spectrum are most applicable to data rates that are significantly smaller than the phase modulator bandwidth. Hence this approach may be useful in reducing discrete spectral components in the Deep Space Network, with modulations in the submegahertz range.

### III. Summary and Conclusions

It has been observed that the spectra of spacecraft downlink telemetry often contain large discrete components at the nulls of the continuous spectrum, which could potentially interfere with adjacent channel signals from other spacecraft signals. This can be attributed to the phase modulator that applies the preprocessed and filtered data stream onto the X-band carrier, modulo  $2\pi$ . The constant envelope property of the transmitted BPSK and OQPSK signals results in the generation of positive-going pulses in the I component, which translates to large discrete components in the spectrum of the transmitted signal, as described in the text.

In this article, a mathematical model of the filtered phase-modulated signal was developed based on the complex envelope of the transmitted signal, and both time-series and complex-plane descriptions of the transmitted signals were analyzed. Techniques designed to reduce



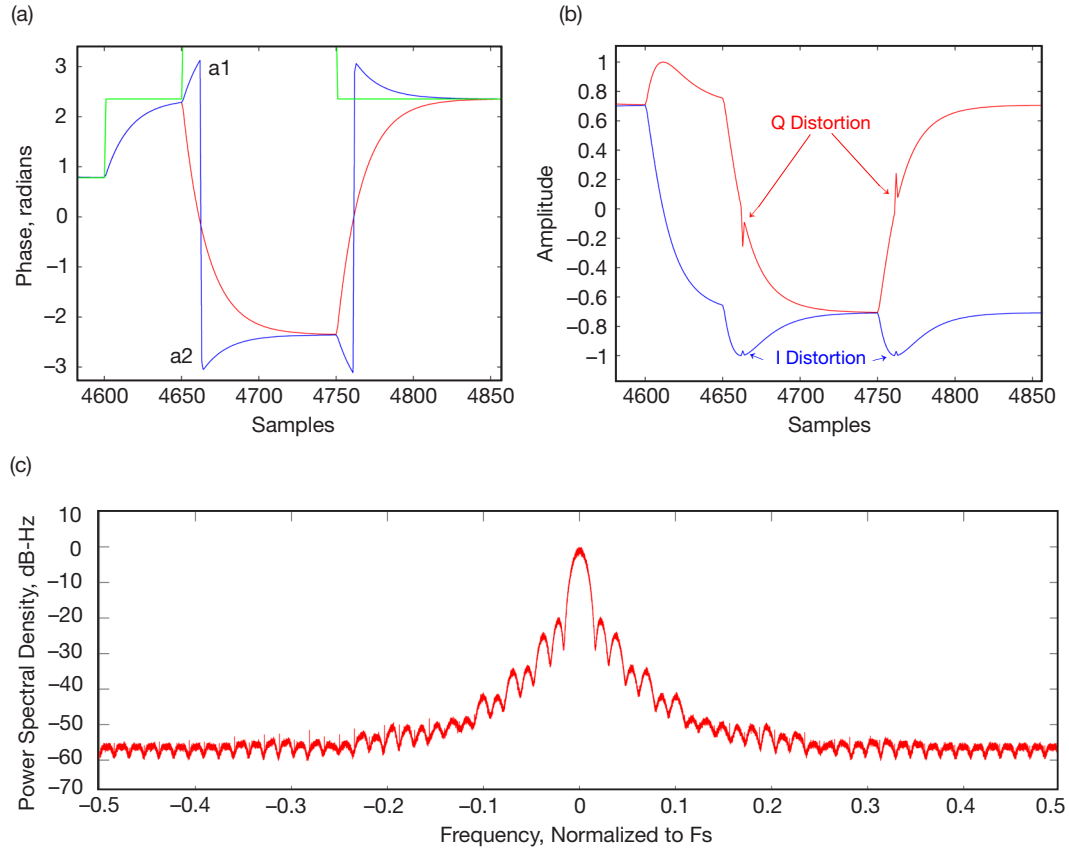


**Figure 20. (a) Wideband-filtered phase waveform to simulate phase modulator response, showing slight distortion at point a2; (b) distortion in the I and Q waveforms due to wideband filtering of phase waveform; (c) spectrum showing small discrete spectral components resulting from positive-going glitches in the I component.**

the magnitude of the discrete components were described and validated via detailed simulations. The results show that the application of Methods 1–4, consisting of phase toggling, phase unwrapping, reflection at predetermined phase boundaries, and detrending, yields reductions of 25 dB or more in the discrete components of transmitted BPSK and OQPSK signals, thus minimizing the possibility of interference from adjacent channel signals when multiple spacecraft signals are received.



## References

- [1] M. K. Simon, "On the Power Spectrum of Angle-Modulated Phase-Shift-Keyed Signals Corrupted by Intersymbol Interference," *The Telecommunications and Data Acquisition Progress Report*, vol. 42-131, Jet Propulsion Laboratory, Pasadena, California, pp. 1–10, November 15, 1997.  
[http://ipnpr.jpl.nasa.gov/progress\\_report/42-131/131B.pdf](http://ipnpr.jpl.nasa.gov/progress_report/42-131/131B.pdf)
- [2] V. K. Prabhu and H. E. Rowe, "Spectra of Digital Phase Modulation by Matrix Methods," *The Bell System Technical Journal*, vol. 53, no. 5, pp. 899–935, May–June 1974.
- [3] S. A. Gronemeyer and A. L. McBride, "MSK and Offset QPSK Modulation," *IEEE Transactions on Communications*, vol. COM-24, no. 8, pp. 809–820, August 1976.